RSC Advances

PAPER

View Article Online
View Journal | View Issue

Cite this: *RSC Adv.*, 2024, **14**, 37512

Development of flexible Zn/MnO_2 secondary batteries using a fumed silica-doped hydrogel electrolyte†

Wenlong Xiong, [ac] Qiyuan Xie,[a] Haoran Zhang,[a] Md. Asraful Alam, [a] Chenjie Zhu, [*b] Lele Wang[a] and Jingliang Xu [*ac]

Hydrogel electrolytes have received tremendous research interest in designing flexible zinc-ion secondary batteries, making them highly promising for flexible energy storage and wearable electronic devices. Herein, we report a composite hydrogel electrolyte (CHE) prepared using a fumed silica-doped gelatin hydrogel. This electrolyte is specifically designed for use in rechargeable aqueous Zn/MnO_2 batteries (ReAZMBs). Experimental results showed that after fumed silica was added, the porosity and ionic conductivity of the gelatin hydrogel electrolyte increased. Meanwhile, adding fumed silica to the hydrogel electrolyte contributed to reducing self-corrosion and promoting rapid and uniform deposition of zinc ions. When the addition of fumed silica to gelatin was 10 wt%, ReAZMBs with this CHE exhibited a superior rate and cycling performance. More specifically, ReAZMBs with this CHE achieved an initial specific capacity of 150 mA h g^{-1} at a current density of 1.5 A g^{-1} and a capacity retention rate of 67% after 1000 cycles, which was much higher than that of the battery with the pure gelatin hydrogel electrolyte (33%). This was because of the improved interface stability between the zinc anode and electrolyte and the reduced formation of by-products ($3Zn(OH)_2 \cdot ZnSO_4 \cdot 3H_2O$ and $3Zn(OH)_2 \cdot ZnSO_4 \cdot 5H_2O$), according to the results of the charge–discharge test of Zn//Zn symmetric batteries and SEM and XRD characterizations of post-run zinc anodes. In addition, the ReAZMBs with the CHE demonstrated good flexibility and could supply power reliably even when bent.

Received 13th September 2024
Accepted 5th November 2024

DOI: 10.1039/d4ra06602b

rsc.li/rsc-advances

1. Introduction

Stretchable and flexible electronics, such as health monitors, wearable devices and roll-ups, display are extremely popular products in today's society and have attracted a lot of research interest.[1–3] The rigidity of traditional energy storage devices limits the application and development of flexible wearable electronics.[4,5] Flexible batteries can maintain high performance in a bent and deformed state, thus adapting to the requirements of flexible electronics with various shapes.[6,7] Therefore, it is very important to develop advanced flexible batteries with high safety and stability, good flexibility and excellent electrochemical performance.[8,9] Aqueous zinc-ion secondary batteries have attracted extensive attention in recent years owing to their advantages of environmental protection, low cost and high safety.[10–12] Moreover, zinc metal has high theoretical capacity (820 mA h g^{-1} and 5855 mA h cm^{-3}), low redox potential (−0.76 V *vs.* SHE), good Zn/Zn^{2+} reversibility in aqueous solutions, and abundant reserves of zinc, which make aqueous zinc-ion batteries highly promising for various applications in the field of flexible wearable electronics.[13–15]

As the most critical component of flexible zinc-ion batteries, hydrogel electrolytes combine the advantages of both an aqueous electrolyte (such as high ionic conductivity and simple preparation) and solid polymer electrolyte (such as good dimensional stability, good interface stability and high safety).[16–18] Hydrogel electrolytes can alleviate the dendrite formation and side reactions of zinc anodes and present good electrochemical performance and excellent mechanical properties. Various hydrogel electrolytes based on polyvinyl alcohol (PVA),[19] polyacrylic acid (PAA),[20,21] and polyacrylamide (PAM)[22–24] have been developed for zinc-ion batteries. However, the application of these polymers for large-scale aqueous zinc-ion batteries could be limited due to their complicated preparation process, high cost and lack of compatibility with biological systems. In recent years, natural biopolymers, such as gelatin,[25,26] agarose,[27] alginate,[28,29] xanthan gum[30] and cellulose[31] have received extensive attention in fabricating hydrogel electrolytes owing to their environmental friendliness,

[a]*State Key Laboratory of Biobased Transportation Fuel Technology, School of Chemical Engineering, Zhengzhou University, Zhengzhou 450001, PR China. E-mail: xujl@zzu.edu.cn*

[b]*College of Biotechnology and Pharmaceutical Engineering, Nanjing Tech University, Nanjing 211816, PR China*

[c]*Henan Center for Outstanding Overseas Scientists, PR China*

† Electronic supplementary information (ESI) available. See DOI: https://doi.org/10.1039/d4ra06602b

degradable properties and abundant reserves. Gelatin has a variety of polar groups, including amino (–NH_2), carboxyl (–COOH), hydroxyl (–OH), and amide (–CONH–), making it easy to cross link by a hydrogen bond to prepare a hydrogel network.[32] Moreover, the gelatin hydrogel has a smooth surface and low average roughness. The flat surface of the gelatin hydrogel electrolyte can form close contact with the electrode, which is conducive to ion transport and is widely used in aqueous zinc ion secondary batteries.[33] However, the gelatin hydrogel electrolyte has low thermal stability, uneven pore structure and low ionic conductivity, which hinder its further application.[34] Therefore, the modification of gelatin-based hydrogel electrolytes is necessary for the fabrication of flexible zinc-ion batteries with excellent electrochemical performance.

Herein, we prepared a composite hydrogel electrolyte (CHE) from the fumed silica-doped gelatin hydrogel for rechargeable aqueous Zn/MnO_2 batteries (ReAZMBs). According to scanning electron microscopy and electrochemical impedance spectroscopy, the porosity and ionic conductivity of gelatin hydrogels increased after fumed silica was added. ReAZMBs (coin cells) with the CHE containing 10 wt% of fumed silica showed the best rate and cycling performance. The structures and morphologies of zinc anodes after 1000 cycles were studied by XRD and SEM. It has been proven that CHE can relieve the corrosion on zinc anodes and inhibit the growth of zinc dendrites. Meanwhile, the effect of fumed silica on the interfacial stability between the CHE and zinc electrodes was investigated by the charge–discharge test of Zn//Zn symmetric batteries. In addition, the ReAZMBs (flexible cell) with the CHE containing 10 wt% of fumed silica presented good flexibility, worked well at a current density of 1.5 A g^{-1}, and could supply power normally even when bent.

2. Experimental section

2.1. Materials

Ammonium fluoride (NH_4F, 99.99%) was purchased from Shanghai Macklin Biochemical Technology Co., Ltd (Shanghai, China). Potassium permanganate ($KMnO_4$, GR) was purchased from Nanjing Chemical Reagent Co., Ltd (Nanjing, China). Gelatin (gel strength ~100 g Bloom) and manganese sulfate monohydrate ($MnSO_4 \cdot H_2O$, AR) were purchased from Shanghai Aladdin Biochemical Technology Co., Ltd (Shanghai, China). Zinc sulfate heptahydrate ($ZnSO_4 \cdot 7H_2O$, 98%) was purchased from Thermo Fisher Scientific (USA) and fumed silica was purchased from Sigma-Aldrich (USA). *N*-Methyl-2-pyrrolidone (NMP), polyvinylidene fluoride (PVDF, HSV 900, Arkema), and acetylene black were purchased from Shenzhen Kejing Star Technology Company (Shenzhen, China). Zinc foil (99.999% purity; thickness = 0.3 mm) was purchased from Qinghe Jinou Metal Material Co., Ltd (Qinghe, China).

2.2. Preparation of α-MnO_2

The α-MnO_2 was synthesized by applying a hydrothermal method.[35–38] First, 0.4 g of $KMnO_4$ and 3.6 g of NH_4F were added to 160 mL of deionized water, and the mixed solution was transferred to a Teflon-lined autoclave with an internal volume of 200 mL. Then, the autoclave was placed in an oven (DZF6020, Shenzhen Kejingstar Technology Company, China) at 200 °C for 24 h and spontaneously cooled to room temperature. Finally, the resulting brown precipitate was washed several times with deionized water, extracted by suction filtration, and dried in a vacuum oven at 80 °C for 12 h to prepare α-MnO_2 powder. The basic XRD, XPS, and SEM characterizations are shown in Fig. S1 (ESI).†

2.3. Preparation of CHE

The CHE was synthesized by applying the gel–sol method.[39] Fig. 1 shows the synthetic route. 2 g of gelatin was dissolved in 18 g of 1 M $ZnSO_4$ and 0.1 M $MnSO_4$ with stirring at 60 °C. Then, fumed silica was added to the above solution. After stirring for 1 h, the obtained solution was cast in a Teflon mold and then cooled at 0 °C to prepare the initial composite hydrogel. Finally, this composite hydrogel was immersed in 2.5 M $ZnSO_4$ and 0.3 M $MnSO_4$ mixed solution at room temperature for 48 h to prepare the CHE. The amounts of fumed silica were 0.1, 0.2, and 0.3 g, corresponding to CHE-5, CHE-10, and CHE-15, respectively. For comparison purposes, the hydrogel electrolyte without fumed silica was referred to as RHE.

2.4. Preparation of the electrodes and assembly of the battery

α-MnO_2, acetylene black, and PVDF powder with a mass ratio of 7 : 2 : 1 were added to *N*-methyl-2-pyrrolidone (NMP) solvent, stirred for 12 h to form a cathode slurry and coated the cathode slurry on the conductive polyethylene film. Subsequently, it was dried in a vacuum drying oven at 60 °C for 12 h and finally cut into 12 mm discs as the cathode.

The pure zinc foil with a thickness of 0.3 mm was polished with grinding powder, then washed with deionized water and ethanol and finally cut into 12 mm discs as the anode.

The cathode, hydrogel electrolyte, and anode were assembled as coin cells (CR2025). The flexible battery was assembled

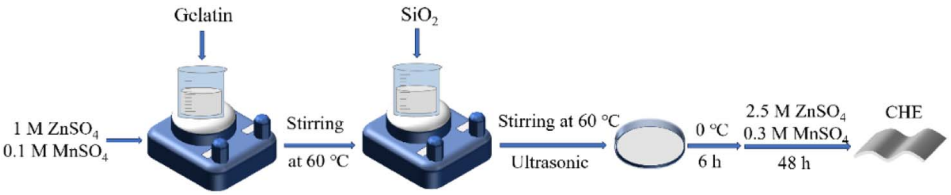

Fig. 1 Schematic of the synthesis route to the CHE.

with a rectangular hydrogel electrolyte and electrodes and finally sealed with a plastic film.

2.5. Material characterizations

The tensile properties of the RHE and CHEs were tested by applying a UTM2502 universal testing machine. The samples were dumbbell-shaped, with a tensile rate of 20 mm min^{-1}. The morphology of RHE and CHE-10 was studied using a field-emission scanning electron microscope (ZEISS, Germany). The composition and microstructure of the zinc anodes after 1000 cycles of the battery were characterized with X-ray diffractometry (Empyrean, The Netherlands) and field-emission scanning electron microscopy (Zeiss, Germany).

2.6. Electrochemical measurements

Electrochemical impedance spectroscopy (EIS) was used to determine the ionic conductivity of the RHE and CHEs on a CHI604E electrochemical workstation (Shanghai Chenhua Instrument Co., China). The test was performed at an open circuit voltage with stainless steel sheets as the blocking electrodes. The ionic conductivity σ of the CHEs was calculated using eqn (1):

$$\sigma = \frac{L}{R_e S}, \quad (1)$$

where R_e (Ω) represents the bulk resistance, S (cm^2) is the contact area between the CHEs and the stainless steel sheets, and L (cm) represents the thickness of the CHEs.

The CHI604E electrochemical workstation received the Tafel curve, electrochemical stability window, chronoamperometry (CA) and hydrogen evolution reaction (HER) curve.

Cyclic voltammetry (CV) was measured on a CHI1040C electrochemical workstation (Shanghai Chenhua Instrument Co., China) at a scan rate of 0.1 mV s^{-1} from 1.0 to 1.9 V.

The nucleation overpotential (NOP) of Zn//Ti batteries was measured using the NEWARE battery tester with constant current discharge at 1 mA cm^{-2} for 1 hour. Then, a constant current charge until the voltage is ≥0.5 V.

The rate performance of the battery was obtained by constant current charge–discharge tests on the battery at current densities from 0.1 A g^{-1} to 5 A g^{-1} using the NEWARE battery tester at room temperature.

Cycling performance was measured with a current density of 1.5 A g^{-1} by the NEWARE battery tester at room temperature.

The RHE and CHE-10 were sandwiched between two zinc sheets to prepare a Zn//Zn symmetric battery, and the battery was tested on the NEWARE battery tester at different current densities.

3. Results and discussion

3.1. Structures and properties of hydrogel electrolytes

As shown in Fig. 2a, all the initial hydrogels were cut into discs with a diameter of 19 mm. Then, they were immersed in a high-concentration solution (2.5 M $ZnSO_4$ + 0.3 M $MnSO_4$) to prepare different hydrogel electrolytes. All the initial hydrogels shrink due to the osmotic pressure. With the increase in the dosage of

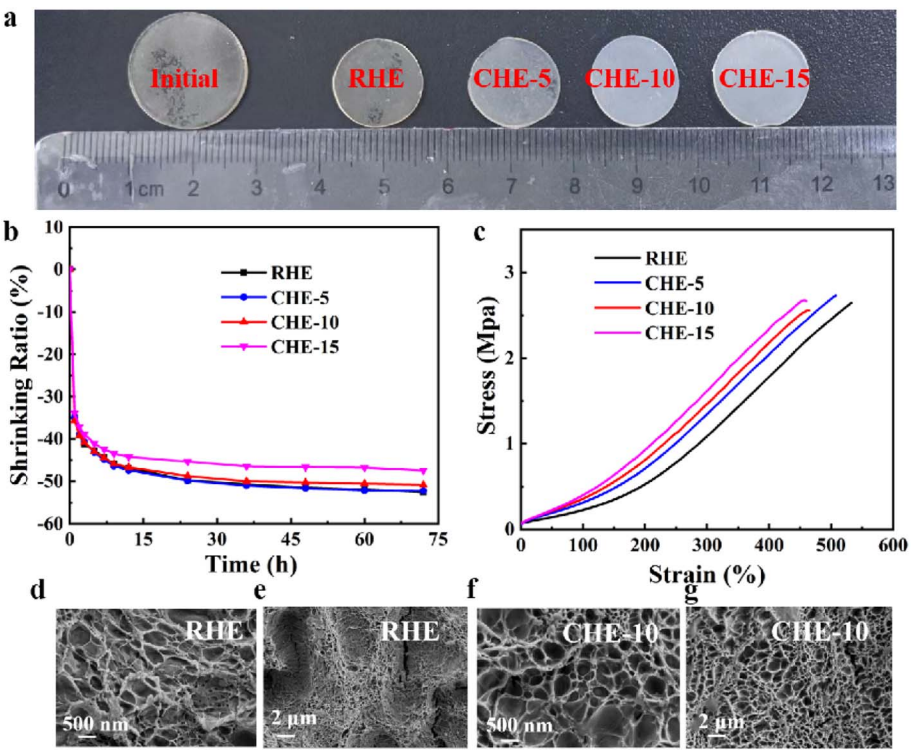

Fig. 2 (a) Optical images of different hydrogel electrolytes. (b) Shrinking ratios of different hydrogel electrolytes. (c) Stress–strain curves of different hydrogel electrolytes. (d and e) SEM images of the RHE. (f and g) SEM images of the CHE-10.

fumed silica, the sizes of RHE, CHE-5, CHE-10, and CHE-15 gradually increase. This indicates that the addition of fumed silica can reduce the shrinkage of the hydrogel. Fig. 2b shows that the shrinkage ratio slightly decreases as the content of fumed silica increases, which means that the addition of fumed silica may improve the ability of electrolyte storage of hydrogel. The hydrogel electrolytes had excellent mechanical properties, as shown in Fig. 2c. It can be observed that the maximum tensile strain of the hydrogel electrolyte gradually decreases with an increase in fumed silica content, while the tensile stress is basically unchanged. The slight decrease in tensile strain may be due to the higher storage of aqueous electrolytes in the fumed silica-doped hydrogel electrolytes. The tensile stress values for RHE, CHE-5, CHE-10 and CHE-15 are 2.65, 2.73, 2.55 and 2.66 MPa, respectively, and their tensile strain values are 532, 508, 465 and 460%, respectively. Compared with the published works (Table S1, ESI†), the mechanical properties of all the prepared hydrogel electrolytes well meet the requirements of assembling Zn/MnO_2 secondary batteries according to the experiments. Compared to the SEM image of the RHE, the SEM image of the representative CHE-10 exhibits superior porous structures with a relatively regular pore structure and high porosity (Fig. 2d–g). This might contribute to a higher capacity for electrolyte storage and faster ion transport.

3.2. Electrochemical behaviour of different hydrogel electrolytes

Fig. 3a shows the EIS of hydrogel electrolytes with or without fumed silica. The EC-circuit is used to fit EIS data and then calculate the ionic conductivity (Fig. 3a inset). The ionic conductivities of the prepared CHE-5, CHE-10, and CHE-15 reach 10.12, 10.30, and 11.59 mS cm^{-1}, respectively, which is higher than that of the RHE (4.2 mS cm^{-1}). This may be because the addition of fumed silica increases the porosity of hydrogel and improves the homogeneousness of pore structure, thus steadily promoting ion migration and enhancing the efficiency of ion transport.[34,40] Fig. 3b shows the nucleation overpotential of different hydrogel electrolytes. A higher nucleation overpotential means a higher nucleation driving force, which is conducive to promoting denser and more uniform Zn deposition, thereby suppressing the formation of dendrites.[41] Compared with RHE (34.21 mV), the addition of fumed silica increases the nucleation overpotential, and the nucleation overpotentials of CHE-5, CHE-10 and CHE-15 reach 65.89, 73.68 and 53.95 mV, respectively. The CHE-10 has the largest nucleation overpotential, which means that it has the best ability to support dense and uniform Zn deposition.[41]

The results of the Tafel test show that CHE-10 has the lowest corrosion current density (Fig. 3c), indicating that CHE-10 could inhibit the self-corrosion of zinc electrodes. According to the HER curves presented in Fig. 3d, the hydrogen evolution voltage of the hydrogel electrolyte is not significantly changed by the addition of fumed silica. CA test was carried out on the symmetric battery to verify the deposition behaviour of zinc ions. As shown in Fig. 3e, the zinc ions in the CHE approach a stable 3D diffusion process rapidly, while a continuous 2D diffusion process of zinc ions in RHE is presented. This means that the addition of fumed silica to the hydrogel electrolyte may contribute to the uniform deposition of zinc ions, leading to a reduction in the formation of zinc dendrites.[42] As shown in Fig. 3f, the addition of fumed silica does not change the electrochemical stability window, and the gelatin hydrogel electrolytes begin to decompose at a voltage range higher than 2.5 V. In

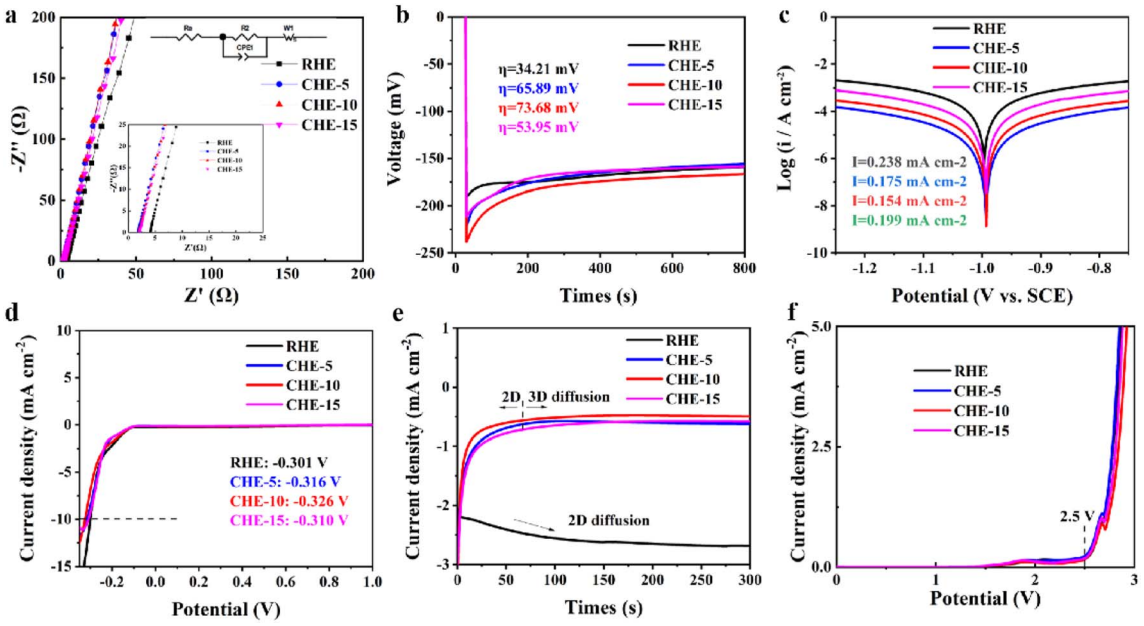

Fig. 3 (a) EIS spectra of different hydrogel electrolytes. (b) Nucleation overpotential of different hydrogel electrolytes. (c) Tafel curves of different hydrogel electrolytes. (d) HER curves of different hydrogel electrolytes. (e) CA curves of different hydrogel electrolytes. (f) Linear sweep voltammetry curves of different hydrogel electrolytes.

fact, the voltage range of Zn/MnO_2 secondary batteries is less than 1.9 V. Therefore, the gelatin hydrogel electrolytes highly meet the needs of Zn/MnO_2 secondary batteries. The above electrochemical tests show that the addition of fumed silica to gelatin hydrogel electrolytes can improve the controllability of the electrochemical behaviour of zinc ions, in which CHE-10 has the best electrochemical performance.

3.3. Electrochemical performance of the batteries

Fig. 4a and b and S2 (ESI)† showed the CV curves of the battery at a scan rate of 0.1 mV s^{-1}. The first scan reveals a strong reduction peak at 1.14 V, followed by a stronger oxidation peak at 1.6 V. In the subsequent scans, two pairs of oxidation/reduction peaks appeared, which correspond to the insertion/extraction of H^+ or Zn^{2+} in α-MnO_2.[28] The redox peaks at 1.23/1.60 V correspond to the insertion/extraction of Zn^{2+}, and the redox peaks at 1.35/1.71 V correspond to the insertion/extraction of H^+. This result shows that fumed silica has no obvious influence on the chemical reaction mechanism of the battery. The charge/discharge profiles of the battery with different electrolytes are shown in Fig. 4c, d and S3 (ESI).† All the charge/discharge curves have two voltage plateaus corresponding to the insertion/extraction of H^+ or Zn^{2+} in α-MnO_2.[28] In the discharge curves, the voltage plateau near 1.23 V is assigned to the insertion process of Zn^{2+}, and the voltage plateau near 1.35 V belongs to the insertion process of H^+. In the charge curves, the voltage plateau near 1.60 V is assigned to the extraction process of Zn^{2+}, and the voltage plateau near 1.71 V belongs to the extraction process of H^+. This is consistent with the corresponding CV curves.

Fig. 4e shows the rate performance of the battery using different electrolytes from 0.1 to 5 A g^{-1}. The discharge specific capacity of the battery using CHE-10 at current densities of 0.1, 0.2, 0.5, 1, 2, 3, and 5 A g^{-1} are 324, 230, 200, 144, 101, 83, and 61 mA h g^{-1}, respectively, which are higher than those of the battery using RHE. This result indicates that fumed silica enhances the discharge specific capacity of gelatin hydrogel electrolytes. When the current density returns to 0.1 A g^{-1}, the discharge specific capacities of the batteries are a little higher than the initial ones, which indicates that the batteries exhibit good reversibility. The higher capacities may be due to the electrodes being gradually activated as the current density returns to 0.1 A g^{-1}.[43]

The cycling performance of the battery using different electrolytes at a current density of 1.5 A g^{-1} for 1000 cycles is shown in Fig. 4f. It can be observed that the initial specific capacity of the battery is about 150 mA h g^{-1}, and then the specific capacity starts to decay, which may have been caused by the dissolution of the cathode, evaporation of water, and corrosion of the zinc anode.[44] Impressively, the ReAZMBs using CHE-10 exhibit good long-term cycling performance by maintaining a capacity of 100 mA h g^{-1} after 1000 cycles, which is much higher than that of battery using RHE (55 mA h g^{-1}). Moreover, considering the factors of cycle number, current density, and discharge capacity, the $Zn//MnO_2$ battery performance in this study is pretty good compared with the published works in the past two years (Fig. S4 and Table S2, ESI†). This outstanding cycling performance is mainly due to the high ionic conductivity of CHE-10, its porous three-dimensional structure, and its good compatibility with electrodes. Therefore, the introduction of fumed silica to the gelatin hydrogel electrolyte can significantly improve the electrochemical performance of the ReAZMBs, especially when the dosage of fumed silica to gelatin is 10 wt% (CHE-10), which is consistent with the results of electrochemical tests.

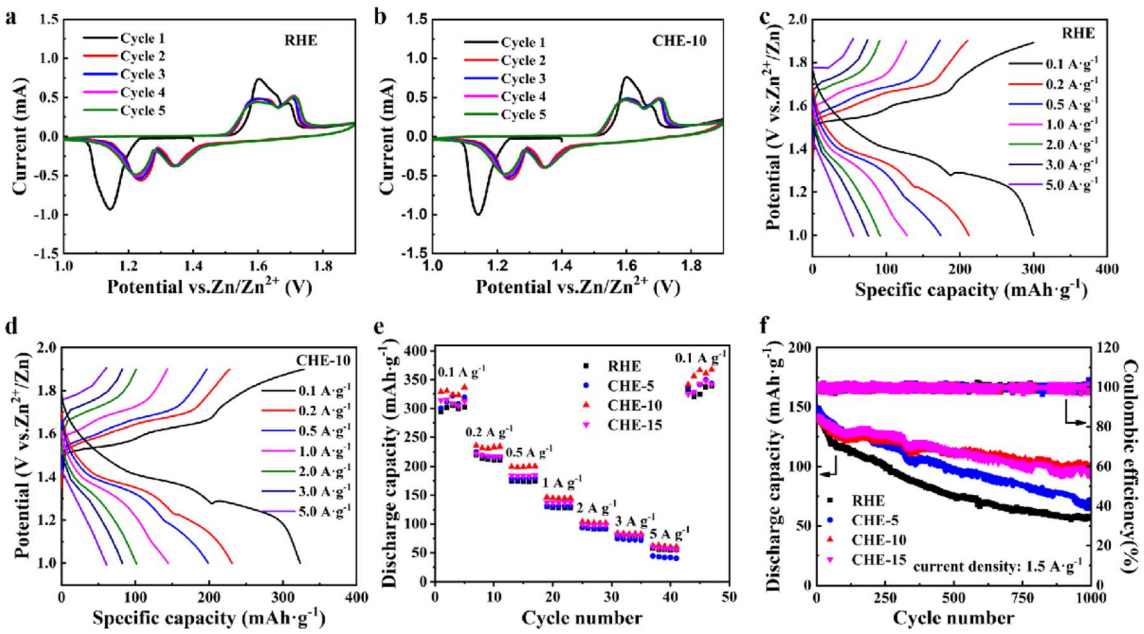

Fig. 4 Electrochemical performance of batteries using different electrolytes: (a and b) cyclic voltammograms. (c and d) Charge/discharge profiles. (e) Rate performance. (f) Cycling performance.

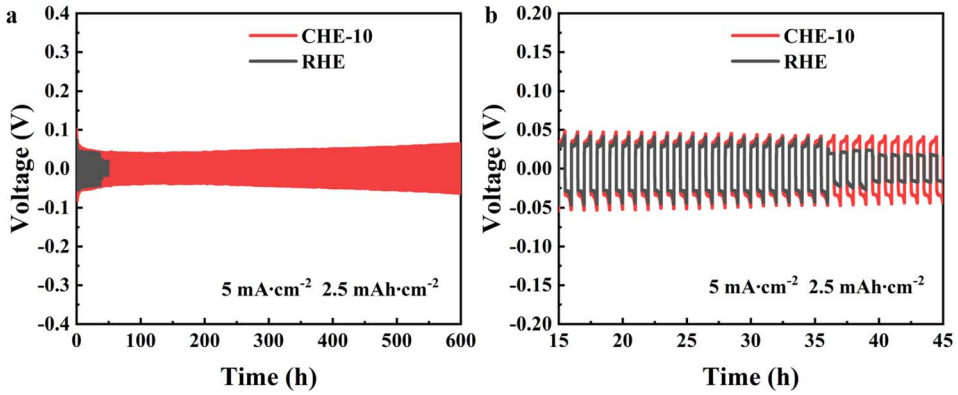

Fig. 5 (a) Polarization curves of Zn//Zn symmetric batteries using RHE and CHE-10. (b) Enlarged voltage profiles of 15 to 45 h.

3.4. Performance of the Zn//Zn symmetric batteries

To investigate the effect of electrolytes on the reversibility and stability of Zn anode, Zn//Zn symmetric batteries were assembled with RHE and CHE-10 for constant current charge and discharge tests.[45] As shown in Fig. 5a and b, the Zn//Zn symmetric battery using CHE-10 can operate stably for 600 hours at a high current density of 5 mA cm^{-2} with a plating capacity of 2.5 mA h cm^{-2}, while the symmetric battery using RHE has a short circuit after 36 hours of operation. This indicates that the symmetric battery using CHE-10 shows more stable and long-term cycle performance than the symmetric battery using RHE. Therefore, the CHE-10 could enhance the compatibility and stability between the gelatin hydrogel electrolyte and the Zn anode, thus further improving the cycling stability of the battery.

3.5. Characterization of the anodes

After 1000 cycles of the battery, the characterization of the anodes by XRD and SEM is shown in Fig. 6. The post-run battery is in the charging state, that is, the state of Zn^{2+} deposition.[46,47] As shown in Fig. 6a, the XRD diffraction peaks of the zinc anode with different electrolytes are in the same position as the initial

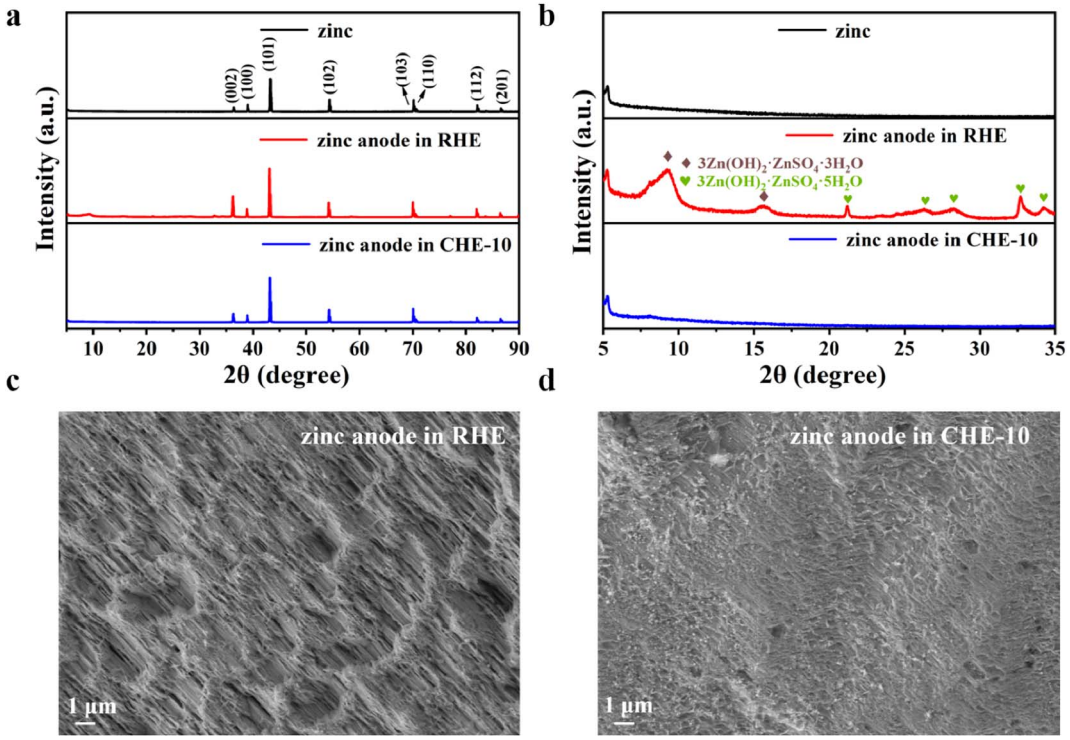

Fig. 6 Characterization of the anodes: (a) XRD patterns of zinc anodes of batteries using the RHE and CHE-10 after 1000 cycles at 1.5 A g^{-1}. (b) Partial enlarged views ($2\theta = 5–35°$) of the XRD patterns. SEM images of the corresponding zinc anodes of batteries using (c) RHE and (d) CHE-10 after 1000 cycles at 1.5 A g^{-1}.

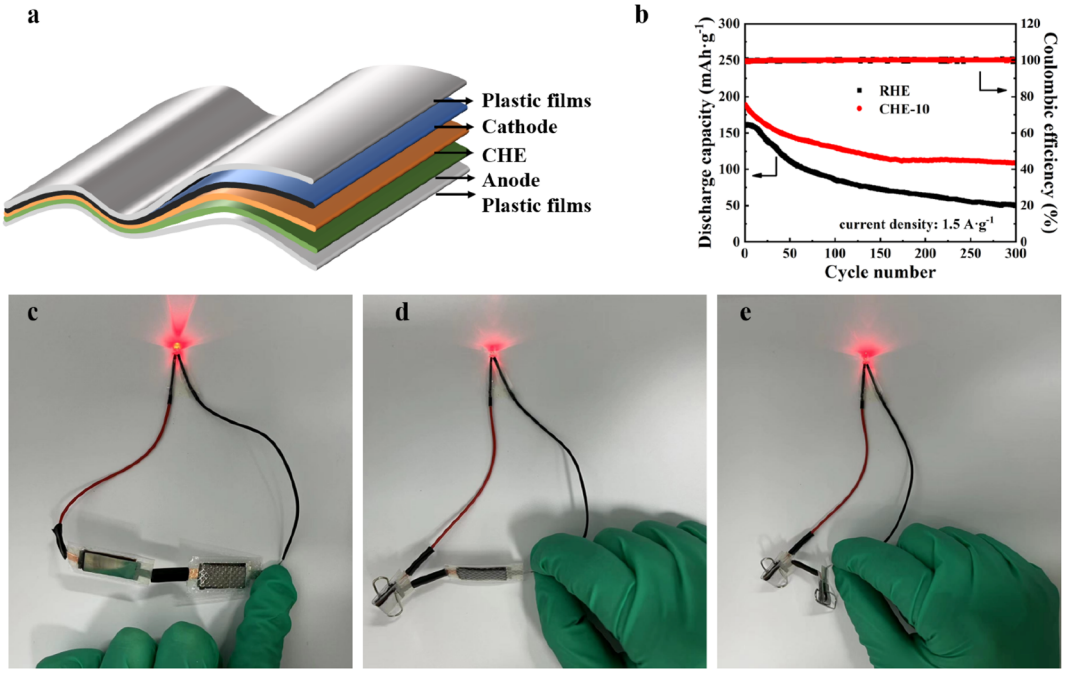

Fig. 7 (a) Schematic of flexible battery. (b) Cycling performance of a flexible battery using different electrolytes. (c–e) Bending test of the flexible battery.

zinc diffraction peaks.[37] However, some newly generated diffraction peaks are detected between $2\theta = 5$–$35°$ in the zinc anode of battery using RHE, and these peaks belong to the by-products, namely $3Zn(OH)_2 \cdot ZnSO_4 \cdot 3H_2O$ (JCPDS no. 39-0689) and $3Zn(OH)_2 \cdot ZnSO_4 \cdot 5H_2O$ (JCPDS no. 39-0688).[48,49] The generation of these by-products tends to corrode the anode.[50] During the long-term operation of the battery, the zinc anode gradually becomes rough and inhomogeneous due to corrosion, which is confirmed by the SEM image shown in Fig. 6c. However, the XRD of the anode of the battery using CHE-10 after cycling is almost the same as that of pure zinc, without the peaks of these by-products, and the SEM pattern presents a flatter surface (Fig. 6d). This indicates that CHE-10 can reduce the by-products during the cycling process and improve the cycling stability of the battery, thus enabling the battery with excellent electrochemical performance.

3.6. Performance of a flexible battery

In Fig. 7a, a schematic diagram of the flexible battery assembly with a sandwich structure is presented. A current density of 1.5 A g^{-1} was used for the charge/discharge test. The initial specific capacity of the flexible battery using CEH-10 was 180 mA h g^{-1}, which was higher than that of the flexible battery with RHE. After 300 cycles, the flexible battery with CHE-10 still had a specific capacity of 110 mA h g^{-1}, which is much higher than that of the flexible battery with RHE (50 mA h g^{-1}) (Fig. 7b). As shown in Fig. 7c–e, connecting two flexible batteries using CHE-10 in series can make the 3 V light-emitting diode emit light, and the light-emitting diode can still light up normally after bending the flexible battery by 180°, which indicates that the flexible zinc ion battery prepared with CHE-10 has good resistance to bending and safety. Thus, the ReAZMBs presented in this study have great potential for application in flexible electronic devices.

4. Conclusion

In summary, CHE-10 prepared by fumed silica-doped gelatin hydrogel significantly improves the electrochemical performance of rechargeable aqueous Zn/MnO_2 batteries. CHE-10 can fix water and enhance the interface stability between the zinc electrode and electrolyte, hence preventing the formation of zinc dendrites and other by-products. When comparing batteries using RHE, it is evident that CHE-10 exhibits a superior rate and cycling performance. The initial specific capacity of the battery using CHE-10 reaches 150 mA h g^{-1} at a current density of 1.5 A g^{-1} and maintains a capacity of 100 mA h g^{-1} even after 1000 cycles, which is much higher than the battery using RHE (55 mA h g^{-1}). Simultaneously, the flexible battery also has excellent safety and can still supply power normally when bent at 180°. The low cost, simple preparation, and non-toxicity method offers the possibility of industrial production of CHE-10, which has great potential for application in the field of flexible electronic devices.

Data availability

All data are presented in this article and the ESI,† and raw data is available upon request from the corresponding author.

Conflicts of interest

There are no conflicts of interest to declare.

Acknowledgements

This work was supported by the foundation of the National Natural Science Foundation of China (No. 22278382, 21908205, and 22378195), Innovation Leadership Program in Sciences and Technologies for Central Plains Talent Plan (No. 214200510009), Program for Science & Technology Innovative Research Team in the University of Henan Province (No. 22IRTSTHN007), Young Elite Scientists Sponsorship Program by Henan Association for Science and Technology (No. 2022HYTP018), Key Program of Henan Provincial Science and Technology R&D Plan Joint Fund for Cultivation of Superior Disciplines (No. 222301420008), Henan Provincial Key Research and Development Program (No. 202102210312), and Program of Processing and Efficient Utilization of Biomass Resources of Henan Center for Outstanding Overseas Scientists (No. GZS2022007).

References

1 X. Li, D. Wang and F. Ran, *Energy Storage Mater.*, 2023, **56**, 351–393.
2 Y. Li, J. Fu, C. Zhong, T. Wu, Z. Chen, W. Hu, K. Amine and J. Lu, *Adv. Energy Mater.*, 2018, **9**, 1802605.
3 Z. Wang, Y. Li, J. Wang, R. Ji, H. Yuan, Y. Wang and H. Wang, *Carbon Energy*, 2022, **4**, 411–445.
4 Y. Zeng, J. Liang, J. Zheng, Z. Huang, X. Zhang, G. Zhu, Z. Wang, H. Liang and Y. Z. Zhang, *Appl. Phys. Rev.*, 2022, **9**, 021304.
5 W. Wang, C. Li, S. Liu, J. Zhang, D. Zhang, J. Du, Q. Zhang and Y. Yao, *Adv. Energy Mater.*, 2023, **13**, 2300250.
6 L. Mao, Q. Meng, A. Ahmad and Z. Wei, *Adv. Energy Mater.*, 2017, **7**, 1700535.
7 Y. Zhu, P. Guan, R. Zhu, S. Zhang, Z. Feng, M. Li, T. Wan, L. Hu, Y. Liu, Q. Li, J. Yu and D. Chu, *J. Energy Chem.*, 2023, **87**, 61–88.
8 C. Li, L. Li, B. He, Y. Ling, J. Pu, L. Wei, L. Sun, Q. Zhang and Y. Yao, *Mater. Sci. Eng. R Rep.*, 2022, **148**, 100671.
9 X. Xiao, Z. Zheng, X. Zhong, R. Gao, Z. Piao, M. Jiao and G. Zhou, *ACS Nano*, 2023, **17**, 1764–1802.
10 N. Zhang, Y. R. Ji, J. C. Wang, P. F. Wang, Y. R. Zhu and T. F. Yi, *J. Energy Chem.*, 2023, **82**, 423–463.
11 Q. Chen, X. Lou, Y. Yuan, K. You, C. Li, C. Jiang, Y. Zeng, S. Zhou, J. Zhang, G. Hou, J. Lu and Y. Tang, *Adv. Mater.*, 2023, **35**, 2306294.
12 Q. Li, Y. Zhao, Y. Wang, A. K. Khasraw, Y. Zhao and X. Sun, *Chem. Res. Chin. Univ.*, 2023, **39**, 599–611.
13 Y. Wang and Y. Chen, *Electrochim. Acta*, 2021, **395**, 139178.
14 S. Olidan, J. Kim, K. Y. Cho and S. Yoon, *Electrochim. Acta*, 2024, **476**, 143704.
15 M. Luo, C. Wang, H. Lu, Y. Lu, B. B. Xu, W. Sun, H. Pan, M. Yan and Y. Jiang, *Energy Storage Mater.*, 2021, **41**, 515–521.
16 C. Y. Chan, Z. Wang, H. Jia, P. F. Ng, L. Chow and B. Fei, *J. Mater. Chem. A*, 2021, **9**, 2043–2069.
17 G. Weng, X. Yang, Z. Wang, Y. Xu and R. Liu, *Small*, 2023, **19**, 2303949.
18 R. Wang, H. Zhang, Y. Hu, R. Wang, J. Shen, Y. Mao, Q. Wu and B. Wang, *Electrochim. Acta*, 2023, **459**, 142583.
19 Y. Zeng, X. Zhang, Y. Meng, M. Yu, J. Yi, Y. Wu, X. Lu and Y. Tong, *Adv. Mater.*, 2017, **29**, 1700274.
20 A. M. Gaikwad, A. M. Zamarayeva, J. Rousseau, H. Chu, I. Derin and D. A. Steingart, *Adv. Mater.*, 2012, **24**, 5071–5076.
21 Z. Song, X. Liu, J. Ding, J. Liu, X. Han, Y. Deng, C. Zhong and W. Hu, *ACS Appl. Mater. Interfaces*, 2022, **14**, 49801–49810.
22 Y. Huang, M. Zhong, F. Shi, X. Liu, Z. Tang, Y. Wang, Y. Huang, H. Hou, X. Xie and C. Zhi, *Angew. Chem.*, 2017, **129**, 9269–9273.
23 H. Li, Z. Liu, G. Liang, Y. Huang, Y. Huang, M. Zhu, Z. Pei, Q. Xue, Z. Tang, Y. Wang, B. Li and C. Zhi, *ACS Nano*, 2018, **12**, 3140–3148.
24 H. Dou, M. Xu, Y. Zheng, Z. Li, G. Wen, Z. Zhang, L. Yang, Q. Ma, A. Yu, D. Luo, X. Wang and Z. Chen, *Adv. Mater.*, 2022, **34**, 2110585.
25 Y. J. Jo, K. Y. Kwon, Z. U. Khan, X. Crispin and T. i. Kim, *ACS Appl. Mater. Interfaces*, 2018, **10**, 39083–39090.
26 Z. Yang, Q. Zhang, T. Wu, Q. Li, J. Shi, J. Gan, S. Xiang, H. Wang, C. Hu, Y. Tang and H. Wang, *Angew. Chem. Int. Ed.*, 2024, **63**, e202317457.
27 M. Zhang, J. H. Li, Y. Tang, D. W. Wang, H. Hu, M. Liu, B. Xiao and P. F. Wang, *Energy Storage Mater.*, 2024, **65**, 103113.
28 Y. Tang, C. Liu, H. Zhu, X. Xie, J. Gao, C. Deng, M. Han, S. Liang and J. Zhou, *Energy Storage Mater.*, 2020, **27**, 109–116.
29 B. Zhang, L. Qin, Y. Fang, Y. Chai, X. Xie, B. Lu, S. Liang and J. Zhou, *Sci. Bull.*, 2022, **67**, 955–962.
30 Y. Chen, J. Zhao and Y. Wang, *ACS Appl. Energy Mater.*, 2020, **3**, 9058–9065.
31 M. Chen, J. Chen, W. Zhou, X. Han, Y. Yao and C. P. Wong, *Adv. Mater.*, 2021, **33**, e2007559.
32 X. Hu, K. Liu, S. Zhang, G. Shao, S. R. P. Silva and P. Zhang, *Nano Res.*, 2023, **17**, 2790–2799.
33 Q. Han, X. Chi, S. Zhang, Y. Liu, B. Zhou, J. Yang and Y. Liu, *J. Mater. Chem. A*, 2018, **6**, 23046–23054.
34 H. Li, C. Han, Y. Huang, Y. Huang, M. Zhu, Z. Pei, Q. Xue, Z. Wang, Z. Liu, Z. Tang, Y. Wang, F. Kang, B. Li and C. Zhi, *Energy Environ. Sci.*, 2018, **11**, 941–951.
35 Z. Ma, F. Jing, L. Hou, L. Fan, Y. Zhao, Y. Fan and X. Qin, *Nano*, 2020, **15**, 2050014.
36 J. Xu, X. Hu, M. A. Alam, G. Muhammad, Y. Lv, M. Wang, C. Zhu and W. Xiong, *RSC Adv.*, 2021, **11**, 35280–35286.
37 J. Xu, M. Wang, M. A. Alam, G. Muhammad, Y. Lv, C. Zhu, H. Zhang and W. Xiong, *ACS Sustain. Chem. Eng.*, 2022, **10**, 2063–2071.
38 J. Xu, M. Wang, M. Asraful Alam, T. K. A. Hoang, Y. Zhang, H. Li, Y. Lv, A. Zhao and W. Xiong, *Fuel*, 2023, **333**, 126450.
39 G. Ge, Y. Zhang, J. Shao, W. Wang, W. Si, W. Huang and X. Dong, *Adv. Funct. Mater.*, 2018, 1802576.

40 S. Tang, Q. Lan, L. Xu, J. Liang, P. Lou, C. Liu, L. Mai, Y. C. Cao and S. Cheng, *Nano Energy*, 2020, 71104600.
41 Y. Lv, M. Zhao, Y. Du, Y. Kang, Y. Xiao and S. Chen, *Energy Environ. Sci.*, 2022, **15**, 4748–4760.
42 C. Y. Li, J. L. Wang, D. T. Zhang, M. P. Li, H. Chen, W. H. Yi, X. Y. Ren, B. Liu, X. F. Lu and M. C. Liu, *J. Energy Chem.*, 2024, **97**, 342–351.
43 Y. Huang, J. Zhang, J. Liu, Z. Li, S. Jin, Z. Li, S. Zhang and H. Zhou, *Mater. Today Energy*, 2019, **14**, 100349.
44 X. Zeng, J. Liu, J. Mao, J. Hao, Z. Wang, S. Zhou, C. D. Ling and Z. Guo, *Adv. Energy Mater.*, 2020, **10**, 1904163.
45 D. Han, Z. Wang, H. Lu, H. Li, C. Cui, Z. Zhang, R. Sun, C. Geng, Q. Liang, X. Guo, Y. Mo, X. Zhi, F. Kang, Z. Weng and Q. H. Yang, *Adv. Energy Mater.*, 2022, **12**, 2102982.
46 C. Deng, X. Xie, J. Han, Y. Tang, J. Gao, C. Liu, X. Shi, J. Zhou and S. Liang, *Adv. Funct. Mater.*, 2020, **30**, 2000599.
47 K. E. K. Sun, T. K. A. Hoang, T. N. L. Doan, Y. Yu, X. Zhu, Y. Tian and P. Chen, *ACS Appl. Mater. Interfaces*, 2017, **9**, 9681–9687.
48 Y. Deng, Y. Wu, L. Wang, K. Zhang, Y. Wang and L. Yan, *J. Colloid Interface Sci.*, 2023, **633**, 142–154.
49 K. Wang, T. T. Su, C. Y. Shao, W. F. Ren and R. C. Sun, *ACS Sustain. Chem. Eng.*, 2022, **10**, 16225–16237.
50 C. Li, X. Xie, S. Liang and J. Zhou, *Energy Environ. Mater.*, 2020, **3**, 146–159.